IEEE Photonics Journal
An IEEE Photonics Society Publication

Open Access

Highly Nondegenerate Four-Wave Mixing in Single-Mode Fabry–Pérot Laser Diode Subject to Dual-Mode Injection

Volume 8, Number 2, April 2016

Jian-Wei Wu
Bikash Nakarmi
Yong Hyub Won

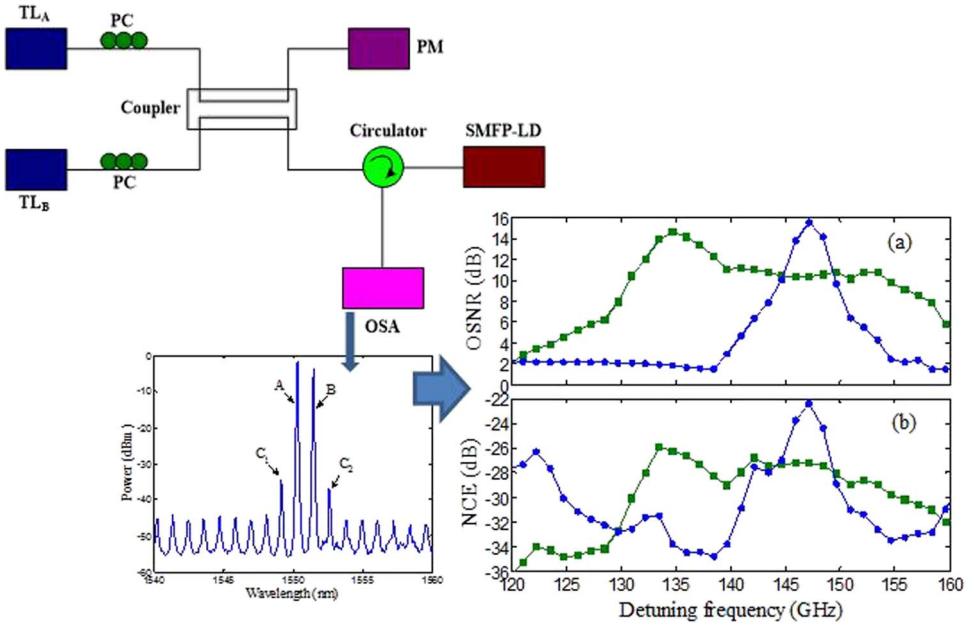

DOI: 10.1109/JPHOT.2016.2539599
1943-0655 © 2016 IEEE

IEEE photonics SOCIETY

IEEE

Highly Nondegenerate Four-Wave Mixing in Single-Mode Fabry–Pérot Laser Diode Subject to Dual-Mode Injection

Jian-Wei Wu,[1,2] Bikash Nakarmi,[3] and Yong Hyub Won[3]

[1]College of Physics and Electronic Engineering, Chongqing Normal University, Chongqing 401331, China
[2]State Key Laboratory of Millimeter Waves, Southeast University, Nanjing 210096, China
[3]School of Electrical Engineering, Korea Advanced Institute of Science and Technology, Daejeon 305-714, South Korea

DOI: 10.1109/JPHOT.2016.2539599

Manuscript received January 17, 2016; revised March 2, 2016; accepted March 4, 2016. Date of publication March 8, 2016; date of current version March 24, 2016. This work was supported in part by the National Natural Science Foundation of China under Grant 61205111; by the Open Foundation of State Key Laboratory of Millimeter Waves under Grant K201513; by the Open Foundation of State Key Laboratory of Advanced Optical Communication Systems and Networks, China; and by the West Project of China Scholarship Council under Grant 201408505054. Corresponding author: Y. H. Won (e-mail: yhwon@kaist.ac.kr).

Abstract: In this paper, highly nondegenerate four-wave mixing (NDFWM) resulting from external dual-mode injection (pump–probe structure) in the single-mode Fabry-Pérot laser diode (SMFP-LD) is proposed and experimentally demonstrated. To cause the effective NDFWM process, both pump and probe beams with enough power levels should, respectively, be close to various resonance modes in the active region, whose detuning frequency can be discontinuously varied from more than 100 GHz to up to 800 GHz. Normalized conversion efficiency (NCE) and optical signal-to-noise ratio (OSNR) of newly generated conjugate signals are strongly dependent on external injection power, wavelength detuning, and detuning frequency. In addition, the NDFWM process exhibits injection probe power-related hysteresis behaviors, whereas the input power and wavelength for pump beam are, respectively, fixed at some special constants.

Index Terms: Nonlinear optics, laser diode, four-wave mixing, conversion efficiency, bistability.

1. Introduction

Four-wave mixing (FWM) process driven by third-order nonlinear susceptibility $\chi^{(3)}$ plays significant roles in some optical elements, which has attracted much attention based on various semiconductor lasers (SL) [1]–[4], highly nonlinear fibers [5]–[7], silicon-based waveguides [8]–[10], photonic crystals [11], [12], semiconductor optical amplifiers (SOA) [13]–[15], and other waveguides [16]–[18], owing to its some potential applications for performing the wavelength conversion [19]–[21], optical switching [22], [23], and photonic generation [24]. In previous reports, one can find that FWM related techniques in various materials have prominent advantages and competition abilities, which have also some limitations for applications due to high cost and power consumption. Therefore, it is a very challenging research to explore other devices to overcome these bottleneck factors in nonlinear wave mixing-based technologies. It is lucky that one can

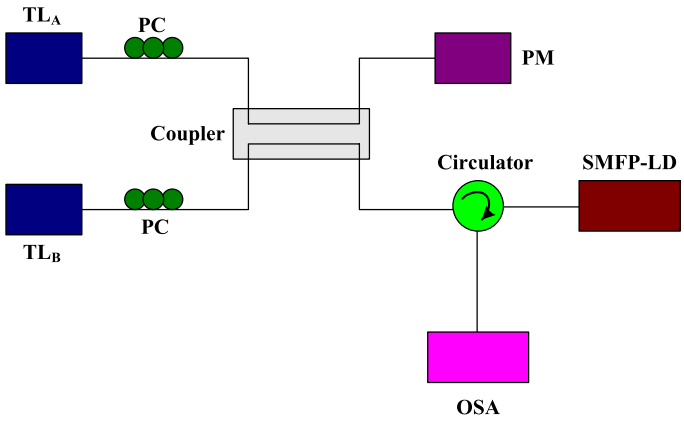

Fig. 1. Experimental setup for NDFWM process in SMFP-LD: TL: Tunable laser, PC: Polarization controller, PM: Power meter, OSA: Optical spectrum analyzer.

know that the single-mode Fabry-Pérot laser diode (SMFP-LD) presented by Won *et al.*, has some significant properties such as compact structure, low cost, self-locking, low threshold, widely tunable range, high side-mode suppression ratio (SMSR), and low power consumption [25]. Over the last decade, the SMFP-LD has been obtained intensive studies by our research group, which is applied to perform many optical functions, including wavelength conversion [26], switching [27], logic gate [28], modulation [29], and flip-flop [30], etc. Even so, nonlinear effects of SMFP-LD should be further presented and discussed to extend its applications. As a result, the highly nondegenerate four-wave mixing (NDFWM) process in SMFP-LD is thoroughly analyzed and investigated in this work, which brings some interesting characteristics attributed to the unique configuration with a built-in external cavity, compared to those in reported results. The normalized conversion efficiency (NCE) and optical signal-to-noise ratio (OSNR) of conjugate signals induced by beating of pump–probe beam are strongly dependent on the detuning frequency between two external injection modes, input wavelengths, and powers that should be judiciously selected to observe obvious FWM signals in the SMFP-LD. Through this study, it is believed that NDFWM effect in SMFP-LD will be useful in the fields of sensors, optical memory, switching, photonic generation, wavelength conversion, and so on.

2. Experimental Setup and Operation Principle

The schematic diagram of experimental setup for NDFWM process in SMFP-LD is displayed in Fig. 1, in which both pump and probe beams are launched through two tunable laser (TL) sources (TL$_A$ and TL$_B$) with 0.01 nm tuning step. The polarization states of output beams are tuned by the polarization controllers (PC), where the TE states of transmission waves are selected to cause the injection locking in SMFP-LD. After the output beams from PC pass through the 50/50 optical fiber coupler, half port is captured by the power meter (PM) to indirectly measure the injection power for SMFP-LD, and the remained beam is coupled into the laser via the optical circulator with 3 dB loss. The output spectrum from SMFP-LD again passes through the circulator and is extracted by the optical spectrum analyzer (OSA) to show outcome FWM spectrum. In experiment, first, only TL$_A$ output as an external pump beam with enough peak power is selected, which is introduced into the SMFP-LD to make it lock at pump wavelength. It is well-known that external injection wavelength should be slightly longer than the adjacent side mode to sufficiently suppress other lasing modes, and the wavelength difference between injection beam and referred side mode is called as the wavelength detuning. The positive (negative) wavelength detuning denotes that the pump wavelength is red-shifted (blue-shifted) compared to the side mode. Of course, it should be noted that, when the wavelength detuning is equal to zero and small negative values, the residual modes and dominated mode can still be suppressed by

the injection beam with proper power, but the locking spectrum is not shifted, compared to the free-running spectrum from SMFP-LD. The mentioned results aren't discussed in this work. Secondly, the pump wave is turned off, and the probe beam launched by TL_B is again injected into the SMFP-LD, which selects another side mode as the referred mode compared with the pump wave. Under the conditions of proper input power and positive wavelength detuning, the laser is again locked at probe wavelength. In experiment, both input powers and wavelengths for pump and probe beams can be easily adjusted by slowly tuning the TL_A and TL_B laser sources. Finally, it is surprising that, after both of continuous laser sources are simultaneously turned on, the NDFWM spectrum can be displayed in the OSA, and properties of the newly generated conjugate signals such as peak, wavelength, conversion efficiency, and optical signal-to-noise ratio can be changed by strictly selecting various injection power and wavelength.

3. Results and Discussion

One can know that nonlinear FWM effect should be attributed to three kinds of nonlinear processes including carrier density pulsation (CDP), spectral hole burning (SHB), and carrier heating (CH). In the case of nearly degenerate FWM with a few GHz detuning frequency defined as the frequency difference between pump and probe waves, the CDP plays a dominated role to cause the new signal generation. Contrarily, while the detuning frequency is up to one terahertz, the intra-band nonlinearities such as SHB and CH are the dominant mechanisms for nonlinear beating of pump and probe beams. However, in this work, the detuning frequency with several hundred GHz is adopted so that all of the referred nonlinear effects should be considered during the NDFWM process [31]. Generally, both normalized conversion efficiency and optical signal-to-noise ratio are used to evaluate the newly generated FWM signals. Here, the corresponding OSNR is defined as the peak power ratio between generated conjugate signal and the nearest side mode [32], and the NCE (η_c) is given by [33]

$$\eta_{c1} = \frac{P_{c1}}{P_{\mathrm{TLA}}^2 P_{\mathrm{TLB}}} \tag{1}$$

$$\eta_{c2} = \frac{P_{c2}}{P_{\mathrm{TLB}}^2 P_{\mathrm{TLA}}} \tag{2}$$

or

$$\eta_{c1} = \frac{P_{c1}}{P_{\mathrm{TLB}}^2 P_{\mathrm{TLA}}} \tag{3}$$

$$\eta_{c2} = \frac{P_{c2}}{P_{\mathrm{TLA}}^2 P_{\mathrm{TLB}}} \tag{4}$$

where P_{c1}, P_{c2}, P_{TLA}, and P_{TLB}, are, respectively, the output powers for conjugate signal C_1, C_2, pump wave, and probe wave, that can be extracted from OSA. The NCE unit in decibels described by the $10 \times \log 10(\eta_C/1\ \mathrm{mW}^{-2})$ is adopted. Frequency of conjugate signal C_1 is larger than that of conjugate signal C_2. While pump wavelength is short (long) compared to the probe wavelength, (1)–(4) are selected to calculate the NCE.

In the cases of 28 mA bias current and 24.3 °C working temperature for active region in the SMFP-LD, the output free-running spectrum with 33.3 dB SMSR is displayed in Fig. 2, in which only one emission mode called as dominated mode is effectively amplified, and other resonance modes are remarkably suppressed. The residual modes whose wavelengths are longer (shorter) than that of dominated mode are orderly counted $+1, +2, +3, \ldots, (-1, -2, -3, \ldots)$. While both pump beam with −4 dBm peak power and 0 wavelength detuning and probe beam with −4.5 dBm peak power and 0.08 wavelength detuning select, respectively, +7 order and +8 order side modes as their referring modes, the output spectrum are, simultaneously, locked at two external injection wavelengths shown in Fig. 3, in which one can see that two lasing modes located at +6 order and +9 order side modes are significantly enhanced, compared to

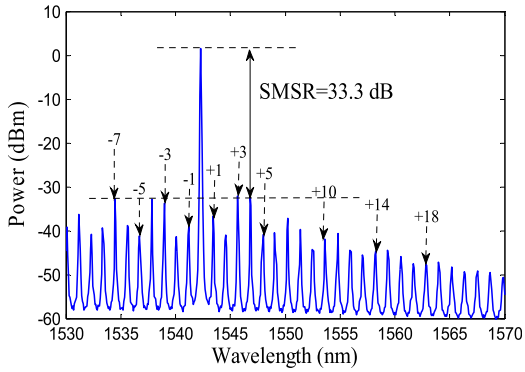

Fig. 2. Free-running spectrum of SMFP-LD with bias current of 28 mA and operation temperature of 24.3 °C.

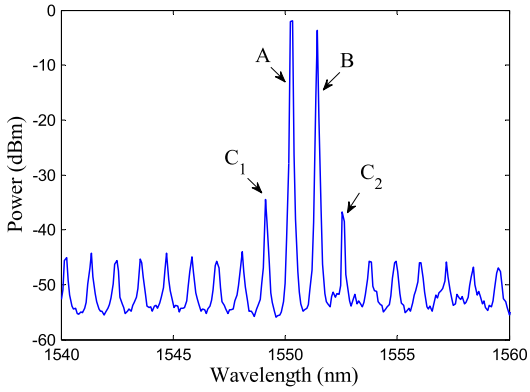

Fig. 3. Optical spectrum of NDFWM process.

other residual side modes. In reality, Fig. 3 is called a typical NDFWM optical spectrum, where the correspondingly enhanced lasing modes labeled C_1 and C_2 are newly generated FWM signals (conjugate signals). The detuning frequency between two injected waves is equal to $\Delta f = f_A - f_B$ (f_A and f_B are the frequencies of pump and probe beams, respectively.) so that frequencies of achieved signal C_1 and signal C_2 are, respectively, shifted to $f_{C1} = f_A + \Delta f$, and $f_{C2} = f_B - \Delta f$. The generation process of FWM signals can be simply described that the beating of pump and probe waves in the active region will induce the dynamic gain and index gratings that scatter the injected pump and probe beams so as to create new conjugate signals [34]. By means of calculations, the NCE and OSNR at conjugate C_1 (C_2) are –26.9 dB (–27.4 dB), and 10.53 dB (8.9 dB), which can be tuned by changing the external injection power and wavelength.

To measure the influence of detuning frequency on the conjugate signals, while the power and wavelength of pump beam, and probe power are kept at the same values given in Fig. 3, various detuning frequencies can be achieved by continuously shifting the probe wavelength around the 8 order side mode. Both NCE and OSNR of the FWM signals are presented against the detuning frequency ranging from 120 GHz to 160 GHz in Fig. 4(a) and (b), where, in the case of 147 GHz detuning frequency, the NCE and OSNR of signal C_2 approach maximum values of about –22 dB and 16 dB that are little higher than those of signal C_1 at 134 GHz detuning frequency. However, detuning frequency related bandwidth for signal C_1 is wider than that of signal C_2. As the spacing of pump–probe beam is less than 140 GHz and up to 155 GHz, the OSNR of signal C_2 is close to zero level, i.e., the corresponding signal is nearly submerged by the residual mode and noise. In contrast, while the detuning frequency is increased from 130 GHz to less than 155 GHz, the signal C_1 is still taking on effective OSNR and NCE, whose

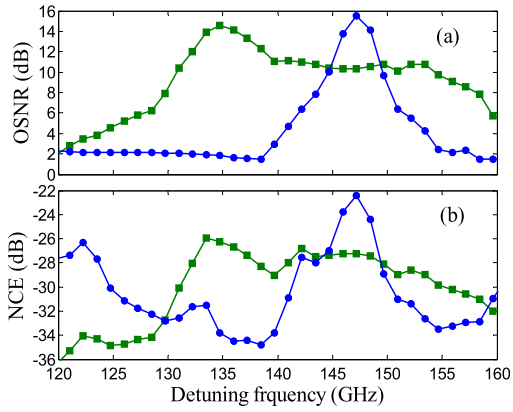

Fig. 4. Conjugate signals change for signal C_1 with green squares and signal C_2 with blue circles with respect to detuning frequency. (a) OSNR and (b) NCE.

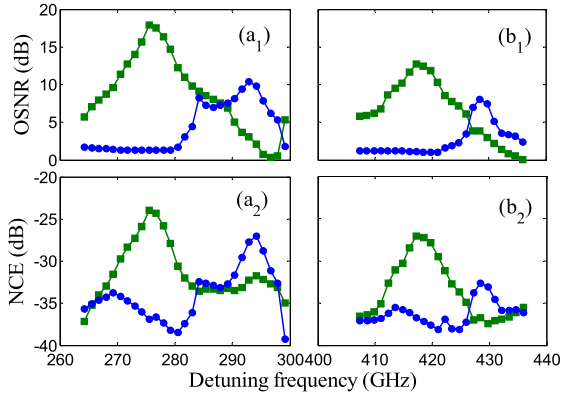

Fig. 5. Conjugate signals change for signal C_1 with green squares and signal C_2 with blue circles as a function of detuning frequency. (a_1, b_1) OSNR with +9, +10 order side mode for probe wave. (b_1, b_2) NCE with +9, +10 order side mode for probe wave.

effective range for conjugate signal C_2 is compressed to about a 5-GHz detuning region. An interesting behavior can be found that the peaks of FWM signals are interactively occurred with the increase of detuning frequency, which is very advantageous to perform wavelength selective switching, and sensor, etc. It is known that the frequency difference of two adjacent lasing modes shown in Fig. 2 is ~140 GHz. As a result, in order to obtain effective FWM process, the shifting of probe wavelength should be around the referred side mode so that the newly generated signals can be resonantly enhanced by the laser cavity. So, it is obvious that the FWM will be completely disappeared as the probe wavelength is apart from the corresponding resonance mode. After the probe beam is sequentially shifted to +9 order and +10 order side modes, the ONSR and NCE of achieved FWM signals has similar trend to the case in Fig. 4 with the increase of detuning frequency, which are plotted in Fig. 5(a) and (b). The beating effect of pump–probe beam is decayed as a result of extended pump–probe spacing so that the frequency dependent bandwidth and outcome power are also reduced. Because the signal C_2 is far from the gain bandwidth of active region, its output power is remarkably low compared to the case of signal C_1 that is close to gain peak. The maximum OSNR and NCE for signal C_1 can, respectively, reach as high as about 19 dB and –24 dB in the case of 275 GHz frequency difference, which are again sunk down to 13 dB and –27 dB for 417 detuning frequency. To this end, one can conclude that, to obtain effective NDFWM interaction, the injected pump and probe beams should be around the resonance modes, and the generated conjugate

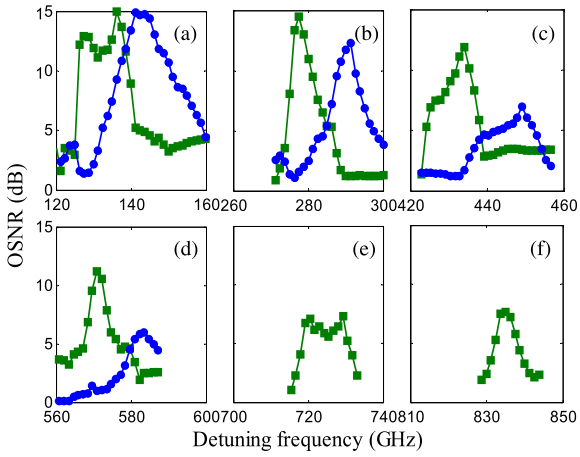

Fig. 6. OSNR of conjugate signal C_1 with green squares and C_2 with blue circles as a function of detuning frequency with various side modes for probe beam. (a) +6, (b) +5, (c) +4, (d) +3, (e) +2, and (f) +1.

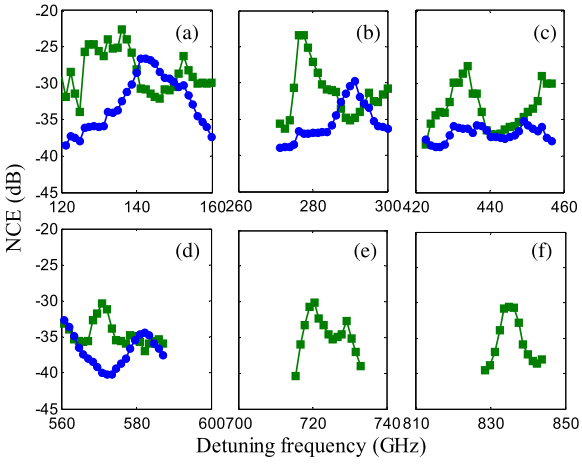

Fig. 7. NCE of conjugate signal C_1 with green squares and C_2 with blue circles as a function of detuning frequency with various side modes for probe beam. (a) +6, (b) +5, (c) +4, (d) +3, (e) +2, and (f) +1.

signals cannot be far from the gain region of the laser. While the probe wave is moved to higher frequency compared with that of pump wave, similar results for OSNR and NCE of FWM signals to those in Fig. 5 are observed in Figs. 6 and 7. The probe wavelength is, orderly, shifted to $+6 \ldots +1$ order side mode position, in which the probe wave is slowly tuned around the referred side mode to observe NDFWM process. It is not difficult to find that the newly grown signals are remarkably decayed in the case of larger detuning frequency. In Fig. 6(e) and (f) and Fig. 7(e) and (f), the conjugate signal C_2 is completely submerged by the noise so that it is not plotted in the figures. The original mechanism for generating conjugate signal is same as above analysis of Fig. 5. However, the conjugate signal C_1 is close to the gain bandwidth with the result that obvious output power can be achieved in the cases of +2 order and +1 order side modes, where NDFWM process is still effective. In addition, the NCE of signal C_1 is significantly higher than that at signal C_2 as the detuning frequency is jumpily increased from about 260 GHz to around 850 GHz. However, in the case of +6 order side mode for probe beam, the maximum output power and bandwidth for two signals are comparable resulting from strong beating effect between pump and probe waves, and the NCE for signal C_2 is lower than that of signal C_1 mainly

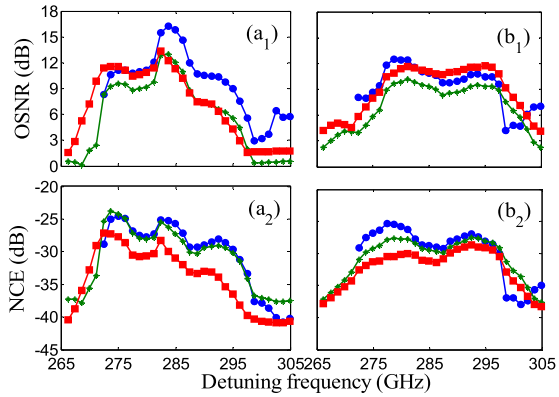

Fig. 8. OSNR and NCE with various injection powers for pump beam (blue lines for −5 dBm, green lines for −3 dBm, and red lines for −1 dBm) in the case of 0.18 nm wavelength detuning for pump beam. OSNR (a_1: signal C_1, b_1: signal C_2). NCE (a_2: signal C_1, b_2: signal C_2).

attributed to higher output pump power. Based on above analysis and parameters values, one can conclude that, under the conditions of effective NDFWM and a determined side mode, signal C_1 is enhanced when the probe beam is moved toward pump wave, i.e., reduced detuning frequency. Contrarily, as the detuning frequency is gradually extended, the signal C_2 is slowly grown and the signal C_1 is suppressed.

To measure the influence of pump power on the NDFWM, Fig. 8 shows the OSNR and NCE of conjugate signals against the detuning frequency with 0.18 nm wavelength detuning, three various input powers for pump beam, and +5 order side mode for probe wave. As the pump power is increased from −5 dBm to −1 dBm that can always lead to the laser locked at pump wavelength. Both the OSNR and NCE of conjugate signals display some difference. In Fig. 8(a_1) and (a_2) for conjugate signal C_1 with −1 dBm pump power level, compared to other two cases of −5 dBm and −3 dBm injection powers, the NCE is decreased due to the increased pump power, and the OSNR bandwidth is slightly broadened owing to the enhanced wave mixing process caused by the high pump power level. However, as the pump power is reduced to −5 dBm level, the signal C_1 can obtain more gain resulting from the reduced carrier consumption at pump beam so that the maximum OSNR is increased to about 17 dB. Of course, it is undoubted that, by further decreasing the injected pump power, the NDFWM process will be disappeared so as to not observe conjugate signals. Obviously, similar results at conjugate signal C_2 are shown in Fig. 8 (b_1) and (b_2). However, it should be pointed out that wavelength of conjugate signal C_1 is close to gain peak so that fluctuations of OSNR and NCE are more remarkable than those of signal C_2. Meanwhile, another interesting behavior is to change the wavelength detuning of pump beam for observing the FWM signals presented in Fig. 9 under a determined −3 dBm pump power condition. As can be seen in this figure, both of conjugate signals have maximum bandwidth in the case of 0.18 nm pump wavelength detuning so that two signals can be simultaneously achieved at the position of same detuning frequency by judiciously shifting the probe wavelength and have relatively flat bandwidth within a large detuning frequency range. However, as the corresponding wavelength detuning is shortened to 0.06 nm and 0 nm, the bandwidth is quickly compressed, and both of newly achieved signals reach, interactively, maximum output with the increase of spacing of pump–probe beam. One can see that the wavelength detuning of pump beam strongly affects the NDFWM effect. Undoubtedly, the behaviors shown in Fig. 9 should have very rich application in all-optical signal processing.

Conjugate signals exhibit injection power related hysteresis behaviors illustrated in Fig. 10, in which different input powers and wavelength detunings for pump beam, and changed wavelength detunings at probe wavelength are, respectively, determined to observe the various bistability phenomena induced by continuously tuning the injection power of probe beam. The input probe power dependent bistability behaviors for OSNR and NCE are displayed,

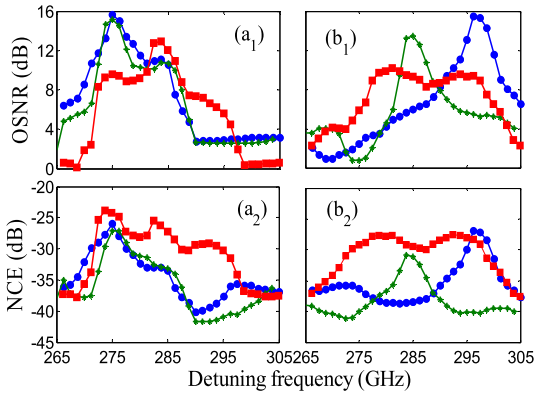

Fig. 9. OSNR and NCE with various wavelength detunings for pump beam (blue lines for 0 nm, green lines for 0.06 nm, and red lines for 0.18 nm) in the case of −3 dBm pump power. OSNR (a_1: signal C_1, b_1: signal C_2). NCE (a_2: signal C_1, b_2: signal C_2).

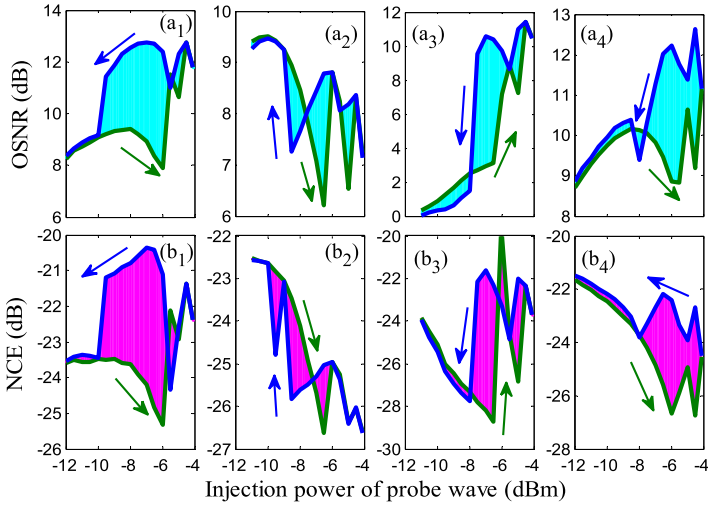

Fig. 10. Hysteresis loops of OSNR (upper row) and NCE (lower row) of conjugate signals as a function of injected probe power. (a_1, b_1) signal C_1 with 0.06 wavelength detuning for probe wave, 0 nm wavelength detuning for pump wave with −3 dBm injection power, (a_2, b_2) signal C_2 with 0.06 nm wavelength detuning for probe wave, 0.12 nm wavelength detuning for pump wave with −1 dBm injection power, (a_3, b_3) signal C_1 with 0.12 nm wavelength detuning for probe wave, 0.12 nm wavelength detuning for pump wave with −1 dBm injection power, (a_4, b_4) signal C_2 with −0.12 nm wavelength detuning for probe wave, and 0 nm wavelength detuning for pump wave with −3 dBm injection power.

respectively, in Fig. 10(a) and (b), in which other parameters adopted such as referred side modes for pump and probe waves are same as those in Figs. 8 and 9. As the probe power is varied between −12 dBm to −4 dBm, the OSNR and NCE of conjugate signals are dependent on the other parameters including wavelength detuning, and input pump power. The OSNR can reach maximum value shown in Fig. 10(a_1), (a_3), and (a_4), except for the case of Fig. 10(a_2), as the injected probe power is increased to about −4 dBm. However, the OSNR shown in Fig. 10(a_2) is up to 9 dB at −10 dBm probe power. Additionally, the hysteresis loops of OSNR and NCE take on obvious butterfly bistabilities in Fig. 10(a_2), and (b_2). However, in other three cases shown in Fig. 10, the counterclockwise bistabilities for OSNR and NCE are plotted in the main region of hysteresis loops, but despite all that, one can see that both

OSNR and NCE have some similar oscillation structure against the probe power, and the widths of achieved hysteresis loops are so wide that it is advantageous to optical memory operation, flip-flop, and sensor technologies, etc., which can be broadened or compressed by adjusting parameter values such as pump power, and wavelength detunings of pump and probe beams.

4. Conclusion

Highly nondegenerate nonlinear four-wave mixing is researched and demonstrated in single-mode Fabry-Pérot laser diode subject to pump–probe injection. As the pump–probe detuning is discontinuously increased from more than 100 GHz to above 800 GHz, newly generated conjugate signals caused by the beating of pump–probe beam are observed, which are strongly dependent on the injection power and wavelength detuning. The conjugate signal at longer wavelength is easily disappeared with the increase of detuning frequency because it is far from the gain bandwidth of gain media. In addition, to efficiently perform the nonlinear NDFWM process, both pump and probe wavelengths should be changed around the corresponding side modes. While the injection wavelength is far from the referred side mode, conjugate signals are submerged by the noise. Finally, the probe power dependent hysteresis phenomena are demonstrated by selecting various operation parameters including wavelength detunings and input pump powers. Through this work, SMFP-LD based NDFWM process can open some potential applications in wavelength conversion, switching, photonic generation, intensity modulation, memory, sensor, and logic gate, that will be presented in future work.

References

[1] A. Mecozzi, A. D'Ottavi, and R. Q. Hui, "Nearly degenerate four-wave mixing in distributed feedback semiconductor lasers operating above threshold," *IEEE J. Quantum Electron.*, vol. 29, no. 6, pp. 1477–1487, Jun. 1993.

[2] G. P. Bava, G. Osella, and P. Debemardi, "Highly nondegenerate four-wave mixing in semiconductor laser oscillators," *Opt. Lett.*, vol. 20, no. 15, pp. 1643–1645, Aug. 1995.

[3] T. Sadeev *et al.*, "Highly efficient non-degenerate four-wave mixing under dual-mode injection in InP/InAs quantum-dash and quantum-dot lasers at 1.55 μm," *Appl. Phys. Lett.*, vol. 107, no. 19, Nov. 2015, Art. no. 191111.

[4] H. Su *et al.*, "Nondegenerate four-wave mixing in quantum dot distributed feedback lasers," *IEEE Photon. Technol. Lett.*, vol. 17, no. 8, pp. 1686–1688, Aug. 2005.

[5] X. Feng *et al.*, "Dispersion-shifted all-solid high index-contrast microstructured optical fiber for nonlinear applications at 1.55 μm," *Opt. Exp.*, vol. 17, no. 22, pp. 20249–20255, Oct. 2009.

[6] S. Asimakis *et al.*, "Towards efficient and broadband four-wave-mixing using short-length dispersion tailored lead silicate holey fibers," *Opt. Exp.*, vol. 15, no. 2, pp. 596–601, Jan. 2007.

[7] K. S. Abedin *et al.*, "Highly nondegenerate femtosecond four-wave mixing in tapered microstructure fiber," *Appl. Phys. Lett.*, vol. 81, no. 8, pp. 1384–1386, Aug. 2002.

[8] H. Fukuda *et al.*, "Four-wave mixing in silicon wire waveguides," *Opt. Exp.*, vol. 13, no. 12, pp. 4629–4637, Jun. 2005.

[9] S. M. Gao, Z. Q. Li, and X. Z. Zhang, "Power-attenuated optimization for four-wave mixing-based wavelength conversion in silicon nanowire waveguides," *J. Electromagn. Waves*, vol. 24, no. 8/9, pp. 1255–1265, Apr. 2012.

[10] S. Azzini *et al.*, "Stimulated and spontaneous four-wave mixing in silicon-on-insulator coupled photonic wire nanocavities," *Appl. Phys. Lett.*, vol. 103, no. 3, Jul. 2013, Art. no. 031117.

[11] T. Y. Gu *et al.*, "Coherent four-wave mixing on hybrid grapheme-silicon photonic crystals," *IEEE J. Sel. Topics Quantum Electron.*, vol. 20, no. 1, Jan./Feb. 2014, Art. no. 7500106.

[12] J. S. Li *et al.*, "Soliton and four-wave mixing effects induced by the third-order dispersion in a photonic crystal fiber with femtosecond pulses pumping at normal-dispersion regime," *IEEE Photon. J.*, vol. 7, no. 5, Oct. 2015, Art. no. 3200211.

[13] P. P. Baveja, D. N. Maywar, and G. P. Agrawal, "Interband four-wave mixing in semiconductor optical amplifiers with ASE-enhanced gain recovery," *IEEE J. Sel. Topics Quantum Electron.*, vol. 18, no. 2, pp. 899–908, Mar. 2012.

[14] O. M. Kharraz, A. B. B. Mohammad, D. I. Forsyth, A. A. Jasim, and H. Ahmad, "Polarization-independent ASE four-wave mixing in a fast semiconductor optical amplifier," *Opt. Commun.*, vol. 355, pp. 498–503, Nov. 2015.

[15] F. X. Li and A. S. Helmy, "All-optical pulse generation based on gain-induced four-wave mixing in a semiconductor optical amplifier," *Opt. Lett.*, vol. 38, no. 8, pp. 1241–1243, Apr. 2013.

[16] P. Apiratikul *et al.*, "Enhanced continuous-wave four-wave mixing efficiency in nonlinear AlGaAs waveguides," *Opt. Exp.*, vol. 22, no. 22, pp. 26814–26824, Oct. 2014.

[17] C. L. Wu *et al.*, "Four-wave mixing in the loss low submicrometer Ta2O5 channel waveguide," *Opt. Lett.*, vol. 40, no. 19, pp. 4528–4531, Oct. 2015.

[18] J. Van Erps *et al.*, "High-resolution optical sampling of 640-Gb/s data using four-wave mixing in dispersion-engineered highly nonlinear As2S3 planar waveguides," *IEEE J. Lightw. Technol.*, vol. 28, no. 2, pp. 209–215, Jan. 2010.

[19] A. Perez-Serrano, J. Javaloyes, and S. Balle, "Multichannel wavelength conversion using four-wave mixing in semiconductor ring lasers," *IEEE Photon. Technol. Lett.*, vol. 25, no. 5, pp. 476–479, Mar. 2013.
[20] J. Chen and S. M. Gao, "Wavelength-assignable 1310/1550 nm wavelength conversion using completely phase-matched two-pump four-wave mixing in a silicon waveguide," *Opt. Commun.*, vol. 356, pp. 389–394, Dec. 2015.
[21] C. Meuer *et al.*, "Cross-gain modulation and four-wave mixing for wavelength conversion in undoped and p-doped 1.3-um quantum dot semiconductor optical amplifiers," *IEEE Photon. J.*, vol. 2, no. 2, pp. 141–151, Apr. 2010.
[22] I. Cestier *et al.*, "Time domain switching/demultiplexing using four wave mixing in GaInP photonic crystal waveguides," *Opt. Exp.*, vol., 19, no. 7, pp. 6093–6099, Mar. 2011.
[23] S. R. Petersen, T. T. Alkeskjold, C. B. Olausson, and J. Lægsgaard, "Polarization switch of four-wave mixing in large mode area hybrid photonic crystal fibers," *Opt. Lett.*, vol. 40, no. 4, pp. 487–490, Feb. 2015.
[24] A. Hurtado, R. Raghunathan, I. D. Henning, M. J. Adams, and L. F. Lester, "Simultaneous microwave- and millimeter-wave signal generation with a 1310-nm quantum-dot-distributed feedback laser," *IEEE J. Sel. Topics Quantum Electron.*, vol. 21, no. 6, Nov./Dec. 2015, Art. no. 1801207.
[25] Y. D. Jeong, Y. H. Won, S. O. Choi, and J. H. Yoon, "Tunable single-mode Fabry-Pérot laser diode using a built-in external cavity and its modulation characteristics," *Opt. Lett.*, vol. 31, no. 17, pp. 2586–2588, Sep. 2006.
[26] M. R. Uddin and Y. H. Won, "All-optical wavelength conversion by the modulation of self-locking state of a single-mode FP-LD," *IEEE Photon. Technol. Lett.*, vol. 22, no. 5, pp. 290–292, Mar. 2010.
[27] B. Nakarmi, T. Q. Hoai, Y. H. Won, and X. P. Zhang, "Short-pulse controlled optical switch using external cavity based single mode Fabry-Pérot laser diode," *Opt. Exp.*, vol. 22, no. 13, pp. 15424–15436, Jun. 2014.
[28] J. W. Wu, B. Nakarmi, Q. H. Tran, and Y. H. Won, "Influence of wavelength detuning on the optical logic gate in side-mode injection locked single-mode Fabry-Pérot laser diode," *Opt. Commun.*, vol. 294, pp. 233–236, May 2013.
[29] J. W. Wu and Y. H. Won, "Temporal response of optical intensity modulation based on side-mode injection locked single-mode Fabry-Pérot laser diode," *J. Opt.*, vol. 15, no. 7, Jul. 2013, Art. no. 075502.
[30] N. L. Hoang, J. S. Cho, Y. H. Won, and Y. D. Jeong, "All-optical flip-flop with high on-off contrast ratio using two injection-locked single-mode Fabry-Pérot laser diodes," *Opt. Exp.*, vol. 15, no. 8, pp. 5166–5171, Apr. 2007.
[31] A. Uskov, J. Mørk, and J. Mark, "Wave mixing in semiconductor laser amplifiers due to carrier heating and spectral-hole burning," *IEEE J. Quantum Electron.*, vol. 30, no. 8, pp. 1769–1781, Aug. 1994.
[32] H. Huang, K. Schires, P. J. Poole, and F. Grillot, "Non-degenerate four-wave mixing in an optically injection-locked InAs/InP quantum dot Fabry-Pérot laser," *Appl. Phys. Lett.*, vol. 106, Apr. 2015, Art. no. 143501.
[33] C. Wang *et al.*, "Nondegenerate four-wave mixing in a dual-mode injection-locked InAs/InP (100) nanostructure laser," *IEEE Photon. J.*, vol. 6, no. 1, Feb. 2014, Art. no. 1500408.
[34] R. Paiella and K. J. Vahala, "Highly nondegenerate four-wave mixing efficiency of an asymmetric coupled quantum well structure," *Appl. Phys. Lett.*, vol. 66, no. 20, pp. 2619–2621, May 1995.